



TECHNICAL ARTICLE

Dynamic Deformation of Low-Alloyed Transformation-Induced Plasticity-Aided Steel from Low to High Strain Rates

Z.Y. Tang, J.N. Huang, H. Ding, and R.D.K. Misra

Submitted: 5 March 2022 / Revised: 14 April 2022 / Accepted: 23 April 2022 / Published online: 11 May 2022

Dynamic deformation behavior of a cold-rolled Fe-1.47Mn-1.40Si-0.21C-0.025Nb transformation-induced plasticity (TRIP)-aided steel was studied at strain rates in the range of 0.01–200 s⁻¹. An understanding of dynamic deformation behavior is important from the perspective of automotive applications and there exists a gap in the knowledge. A novel approach of using a tensile specimen with variable cross section is proposed to realize the controllable strain experiment and study the dynamic deformation process. The study indicated that the increase of adiabatic temperature during dynamic tensile deformation increased the additional mechanical driving force, leading to increase in the stability of retained austenite (RA). The degree of transformation and the rate of transformation of RA during dynamic tensile straining was less than the quasi-static tensile deformation. The microstructure of experimental steel was mainly composed of polygonal ferrite, bainite and RA, and majority of large blocky RA at the ferrite grain boundaries transformed to martensite during the initial stage of dynamic deformation. With the increase of strain, RA with smaller average grain size transformed to martensite. At the end of deformation, only a few small granular RA that was too stable did not transform. With the increase of strain rate from 0.01 to 200 s⁻¹, both yield strength and ultimate tensile strength (UTS) of the experimental steel increased monotonously. However, the total elongation (TEL) initially decreased and then increased. The experimental steel exhibited remarkable mechanical properties with the product of UTS and TEL (PSE) of 25.6 GPa% at strain rate of 200 s⁻¹. The study underscores the significance of strain rate in designing TRIP steel.

Keywords dynamic tensile behavior, mechanical properties, retained austenite stability, TRIP-aided steel

1. Introduction

Transformation-induced plasticity (TRIP) steels, with an outstanding combination of strength and ductility, are excellent candidates for structural applications in the automotive industry (Ref 1-4). The excellent mechanical properties of TRIP steel are mainly due to the TRIP effect, i.e., strain-induced transformation of retained austenite (RA) to martensite, led to the simultaneous increase of strength and ductility (Ref 4-6). To meet the new structural performance requirements, without considerable increase in the automotive mass, TRIP steels are

indispensable (Ref 7, 8). Using TRIP steels to make automotive parts would increase energy absorption ability and improve automotive safety performance (Ref 9-12).

Understanding the dynamic deformation behavior of high strength steels (TRIP steels, medium Mn steel, high Mn steel, etc) is essential for its potential applications (Ref 13-19). Choi et al. (Ref 15) investigated the deformation behavior of low carbon TRIP sheet steels at strain rates in the range of 10⁻³–2.5 × 10² s⁻¹, and indicated that with the increase of strain rates, the yield strength (YS) and ultimate tensile strength (UTS) of the experimental steel was increased. Van Slycken et al. (Ref 16) showed that with the increase of strain rates from 5.6 × 10⁻⁴ to 2 × 10³ s⁻¹, the YS, UTS and total elongation (TEL) of low-alloyed TRIP steels was increased. Wei et al. (Ref 17) studied the dynamic tensile behavior of TRIP-aided steels over wide range of strain rate (400–1600 s⁻¹) and demonstrated that with the increase of strain rates, both YS and UTS of TRIP-aided steels was increased, but the TEL was decreased. They pointed out that the adiabatic temperature rise at high deformation rate increased the stability of retained austenite (RA), resulting in the decrease in the amount of transformed RA. Gao et al. (Ref 18) indicated that when the strain rate was increased from 0.01 to 200 s⁻¹, UTS of Si-Mn TRIP steel was increased, and the TEL first decreased and subsequently increased. Additionally, they demonstrated that the transformation of RA to martensite was not suppressed by adiabatic heating.

He et al. (Ref 19) studied the tensile deformation behavior of Si-Mn TRIP steel over a wide range of strain rate (0.001–

Z.Y. Tang and **H. Ding**, School of Materials Science and Engineering, Northeastern University, Shenyang 110819, China; and Key Laboratory of Lightweight Structural Materials, Shenyang 110819 Liaoning Province, China; **J.N. Huang**, School of Materials Science and Engineering, Fujian University of Technology, Fuzhou 350118, China; and Fujian Provincial Key Laboratory of Advanced Materials Processing and Application, Fuzhou 350118, China; and **R.D.K. Misra**, Laboratory for Excellence in Advanced Steel Research, Department of Metallurgical, Materials and Biomedical Engineering, University of Texas at El Paso, El Paso, TX 79968. Contact e-mails: tangzy@smm.neu.edu.cn, huangjnd@163.com, dmsira2@utep.edu.

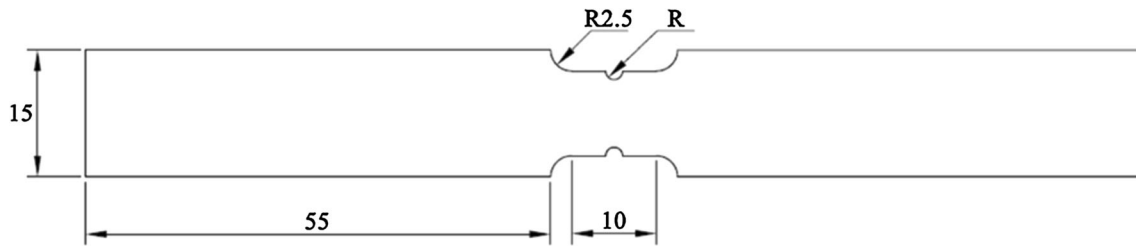


Fig. 1 The dimension of variable cross-section tensile specimen (unit: mm)

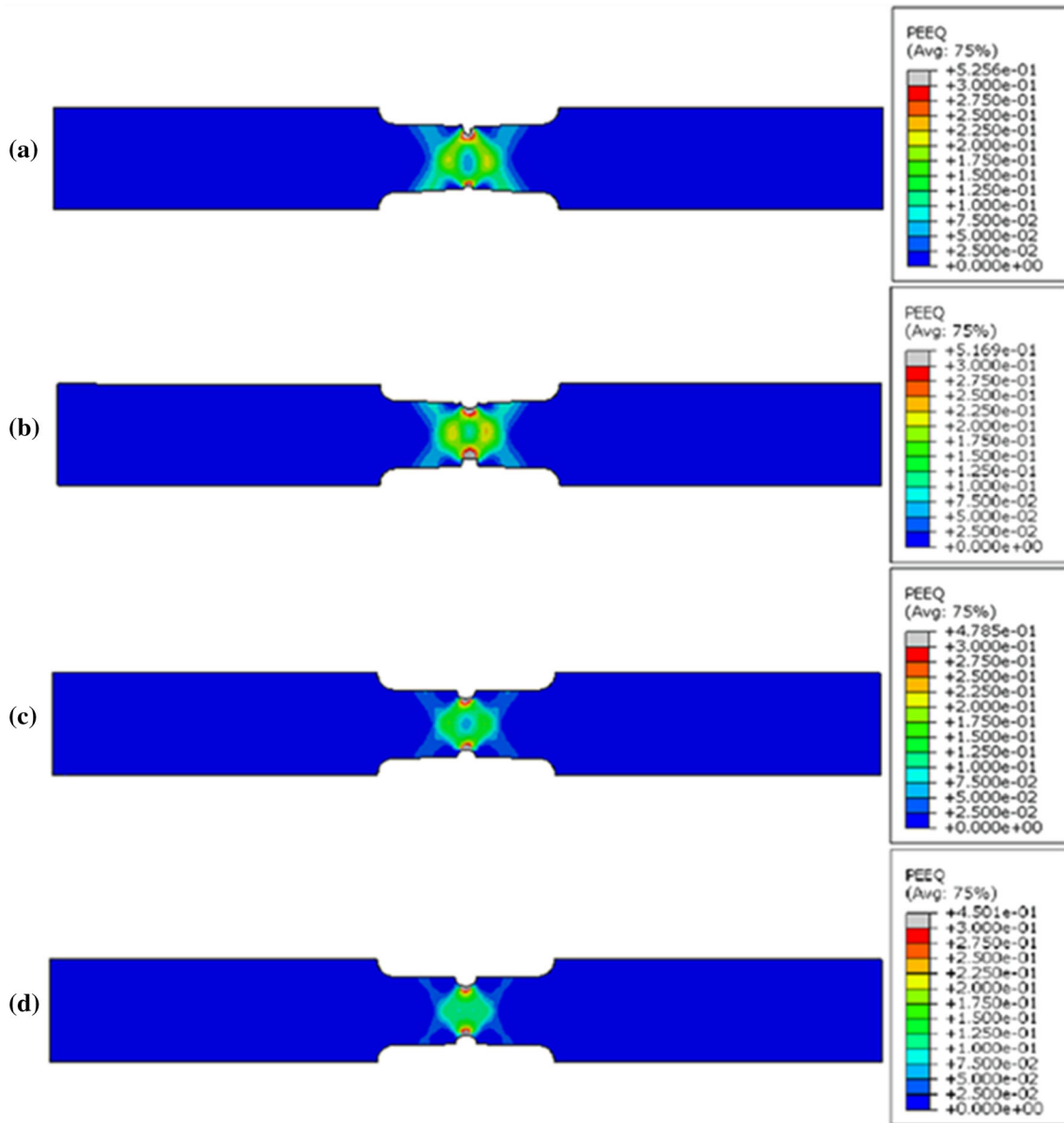


Fig. 2 The strain state of samples with variable cross section simulated by ABAQUS during necking (a) 0.5-sample; (b) 0.75-sample; (c) 1.0-sample; (d) 1.25-sample

2000 s⁻¹), and indicated that the TEL during dynamic tensile straining was always less than that at quasi-static tensile test because the transformation of RA to martensite was inhibited by localized deformation during dynamic tensile test. In general, these studies mainly focused on the dynamic mechanical properties of TRIP steels. However, there are relatively few

studies on the microstructure evolution of TRIP steels deformed at high strain rates. Furthermore, it may be noted from these studies that there is controversy if the adiabatic temperature rise can enhance the stability of RA and inhibit the transformation of RA to martensite. This aspect is unclear and is the focus of the study described here.

In addition, in view of high strain rate, it is difficult to realize the controlled strain experiment to study the transformation process of RA to martensite in TRIP steel during dynamic deformation, which limits our understanding of the behavior of TRIP steels. This also affects the development of stamping technology of TRIP steel and the improvement of anti-collision performance.

Therefore, the mechanical behavior of a high strength low alloy (HSLA) TRIP steel under different strain rates was systematically studied here, and the influence of adiabatic temperature rise on the stability of RA and martensitic transformation under dynamic deformation condition is clari-

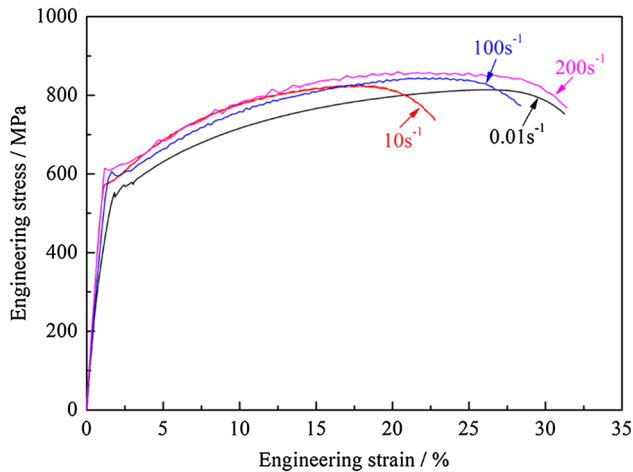


Fig. 3 The engineering stress–strain curve of the experimental steel after tensile deformation at different strain rates

Table 1 Mechanical properties of the experimental steel at different strain rates

Strain rate, s^{-1}	YS, MPa	UTS, MPa	TEL, %	PSE, GPa%
0.01	552	815	29.7	24.2
10	577	825	21.7	17.9
100	590	841	26.6	22.5
200	614	860	29.8	25.6

fied. To elucidate this aspect, an original tensile specimen with variable cross section was designed to realize the controllable strain experiment and study the dynamic deformation process of HSLA TRIP steel, and enhance the understanding of microstructure evolution and plasticity-enhancing mechanism of HSLA TRIP steel during dynamic deformation.

2. Experimental

The nominal chemical composition of the experimental steel was Fe-1.47Mn-1.40Si-0.21C-0.025Nb (in wt.%). The steel was melted in a 50 kg vacuum furnace and cast as ingot. The ingot was heated at 1200 °C for 2 h and hot forged into a rectangular slab of size of 100 × 30 mm, followed by air cooling to room temperature. Then, the forged ingot was soaked at 1200 °C for 2 h and hot rolled to 3 mm thickness by rolling temperature in the range of 1150–900 °C. Finally, the hot rolling sheet was pickled in 20 vol.% HCl solution and cold-rolled to 1 mm thickness.

Two-stage salt bath heat treatment was adopted. First, the experimental steel was annealed at 825 °C for 3 min, and then quenched to the isothermal bainite transformation (IBT) temperature at 410 °C for 3 min, followed by cooling in air to ambient temperature. Tensile specimens had flat dog-bone geometry with a gage length of 10 mm and width of 5 mm were cut from the heat-treated sheet along the rolling direction. Quasi-static tensile tests were performed on SANSMT5000 machine at low strain rate of 0.01 s^{-1} . Dynamic tensile tests were performed on Zwick HTM 5020 machined at different high strain rates (10, 100, 200 s^{-1}). The dimension of variable cross-section tensile specimen is shown in Fig. 1. A circular opening with different radius (0.5, 0.75, 1.0 and 1.25 mm) was made in the middle of the gage length section of tensile specimen to control the cross section of specimen, with the aim to study the dynamic deformation process of TRIP steel under controllable strain. In order to verify the feasibility of variable cross-section specimen tensile method, ABAQUS finite element software was used to simulate the strain condition in different variable cross-section specimens after tensile deformation at strain rate of 100 s^{-1} before high-speed tensile test. As shown in Fig. 2, with the increase of opening depth from 0.5 to 1.25 mm, the strain in the gage section at both the ends of the opening was gradually decreased. This suggested that the

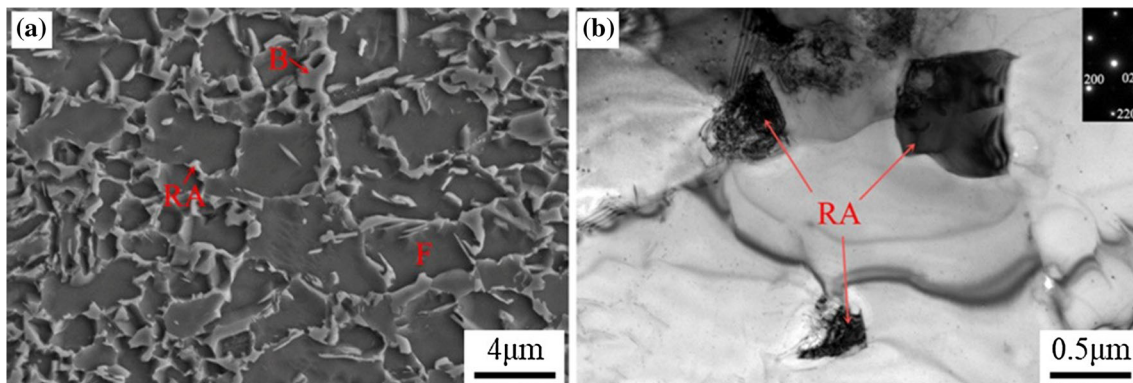


Fig. 4 SEM and TEM micrographs of the experimental steel after two-stage heat treatment: (a) SEM micrograph; (b) TEM micrograph (F: Ferrite, B: Bainite, RA: Retained Austenite)

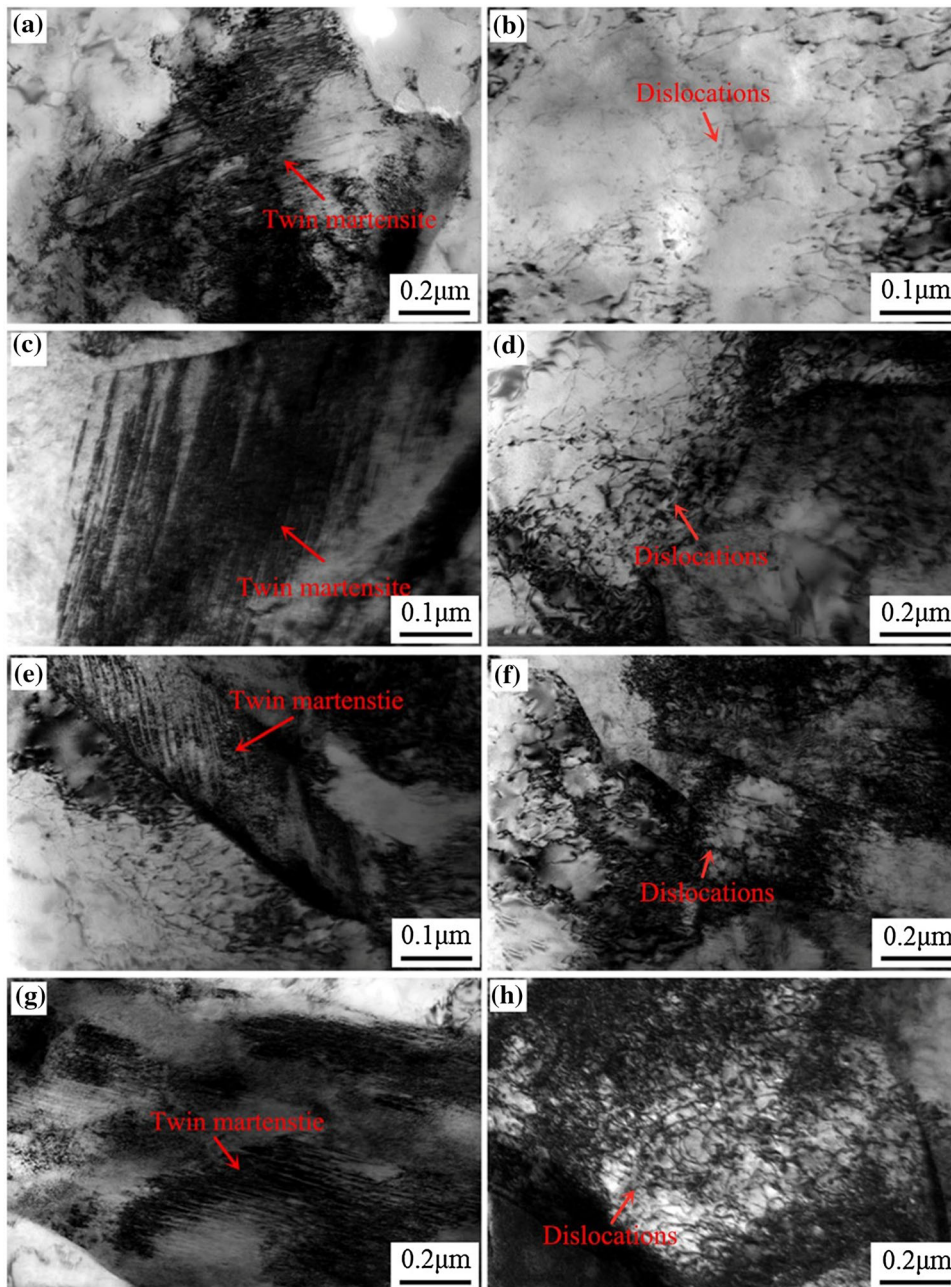


Fig. 5 TEM micrographs of the experimental steel after tensile deformation at different strain rates: (a, b) 0.01 s^{-1} ; (c, d) 10 s^{-1} ; (e, f) 100 s^{-1} ; (g, h) 200 s^{-1}

dynamic deformation process of TRIP steel under controllable strain can be studied by means of variable cross-section specimen tensile method. For convenience, variable cross-section specimens with opening depths of 0.5, 0.75, 1.0 and 1.25 mm are henceforth referred as 0.5-sample, 0.75-sample, 1.0-sample and 1.25-sample, respectively.

In order to minimize the impact of strain state, which was different from area to area, after fracture, the open area was cut, then the specimen for microstructural examination was cut from the middle of the gage length section of tensile specimen. Microstructural examination was carried out by SEM (Zeiss Ultra Plus) equipped with electron backscatter diffraction (EBSD) and TEM (Tecnai G^2 20). The detailed preparations for samples were described in reference (Ref 20). The volume

fraction of RA (V_γ) was determined by XRD (Rigaku, D/Max2250/PC) with CuK_α using direct comparison method (Ref 20).

3. Results

3.1 Mechanical Properties

Figure 3 shows the engineering stress–strain curve of the investigated steel at different strain rates. Some oscillations were observed in the engineering stress–strain curve, which was mainly due to the high-speed tensile test noise. The statistical results of YS, UTS, TEL and the product of UTS and

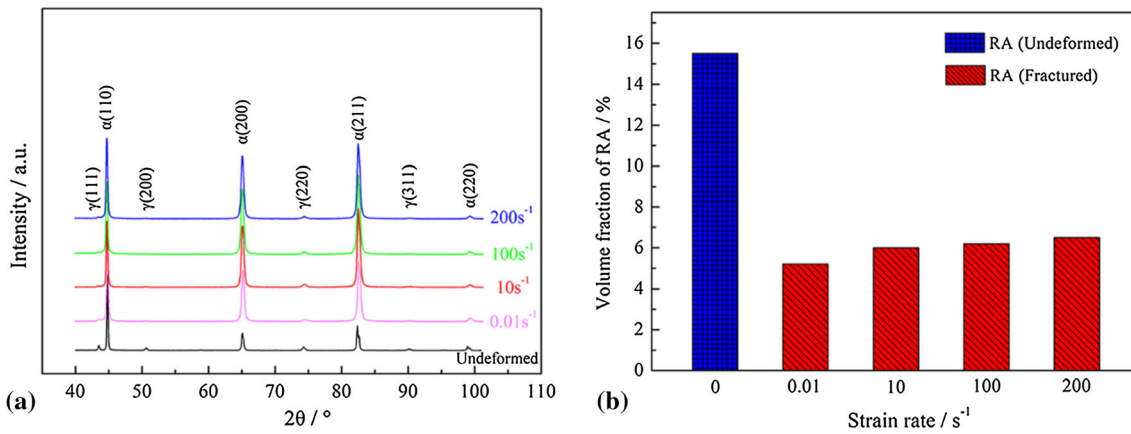


Fig. 6 (a) XRD patterns and (b) measured retained austenite fraction of the experimental steel before and after tensile deformation at different strain rates

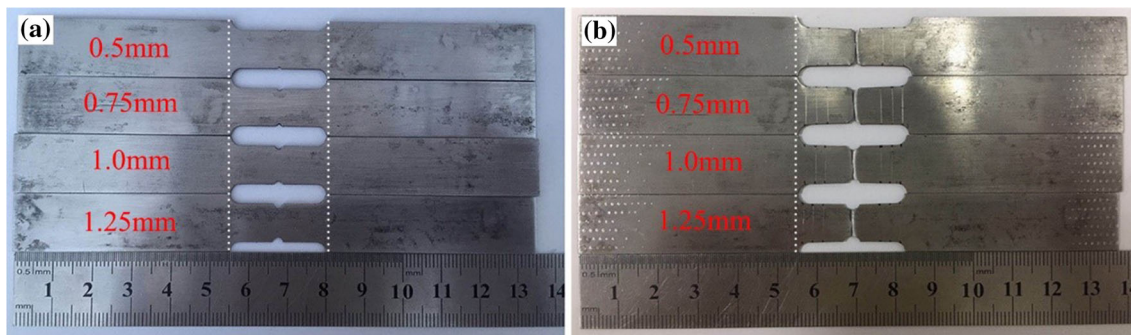


Fig. 7 Macrographs of samples with variable cross section before and after tensile deformation with strain rate of 100 s^{-1} : (a) before tensile deformation; (b) after tensile deformation

TEL (PSE) of investigated steel at different strain rates are shown in Table 1. It can be observed from Fig. 3 and Table 1 that with the strain rate increasing from 0.01 to 200 s^{-1} , the YS and UTS increased monotonously from 552 to 614 MPa and 815 to 860 MPa , respectively. However, the TEL (PSE) first decreased from 29.7 to 21.7% (24.2 - $17.9 \text{ GPa}\%$) with the strain rate increasing from 0.01 to 10 s^{-1} , and then increased to 29.8% ($25.6 \text{ GPa}\%$) when the strain rate was increased to 200 s^{-1} .

3.2 Microstructure

Figure 4 shows SEM and TEM micrographs of experimental steel after two-stage heat treatment. As shown in Fig. 4(a), the microstructure of the experimental steel after two-stage heat treatment consisted of dark gray polygonal ferrite, light gray island bainite, and white granular retained austenite (RA). Some of the blocky RA were located at the ferrite grain boundary, while others were located inside the ferrite grain (Fig. 4b).

Figure 5 shows the TEM micrographs of the experimental steel after tensile deformation at different strain rates. As shown in Fig. 5(a, c, e, g), a number of deformation twins in martensite were present in the experimental steel after tensile deformation at different strain rates, which implied that the TRIP effect occurred during the tensile deformation at different strain rates. Simultaneously, with the strain rate increasing from 0.01 to 1000 s^{-1} , the dislocation density in ferrite was increased and

the density of dislocation tangles and interaction became stronger (Fig. 5b, d, f, h).

Figure 6 shows XRD patterns and volume fraction of RA in the experimental steel before and after deformation at different strain rates. It can be seen from Fig. 6(b) that the RA content in the experimental steel was 15.4% before deformation. After tensile deformation at strain rate of 0.01 , 10 , 100 and 200 s^{-1} , it decreased to 5.2 , 5.4 , 5.7 and 6.2% , respectively. In other words, with the increase of strain rate from 0.01 to 200 s^{-1} , the degree of transformation of RA in steel decreased from 10.2 to 9.2% . It can be deduced that the stability of RA increased with the increase of strain rate.

The variable cross-section specimen tensile method was used to further study the transformation process of retained austenite to martensite in TRIP steel during dynamic deformation. Figure 7 shows the macrographs of the variable cross-section specimen before and after tensile deformation at strain rate of 100 s^{-1} . It can be seen from Fig. 7(b) that the TEL of the samples decreased when the opening depth of the variable cross-section specimen increased from 0.5 to 1.25 mm . The TEL of 0.5 -sample, 0.75 -sample, 1.0 -sample and 1.25 -sample was 18.1 , 10.3 , 8.7 and 5.2% , respectively. Figure 8 shows the EBSD maps of the experimental steel after tensile deformation at strain rate of 100 s^{-1} at various strain levels. The distribution of RA and α -bcc phases are marked in red and blue, respectively. The low angle grain boundaries between 2 and 15 deg are drawn by white lines, the high angle grain boundaries with more than 15 deg misorientation are drawn

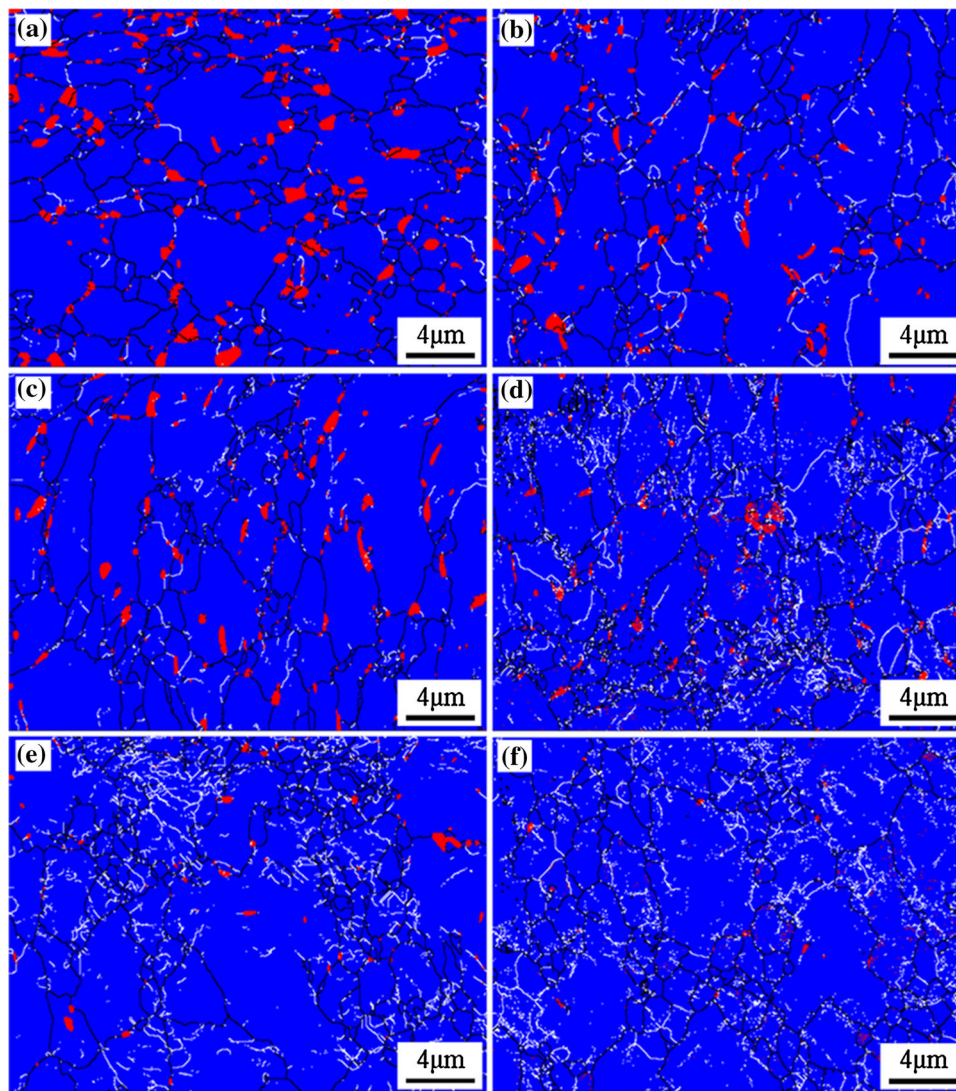


Fig. 8 EBSD maps of the experimental steel after tensile deformation with strain rate of 100 s^{-1} at various strain levels: (a) $\varepsilon = 0$; (b) $\varepsilon = 5.2\%$; (c) $\varepsilon = 8.7\%$; (d) $\varepsilon = 10.3\%$; (e) $\varepsilon = 18.1\%$; (f) $\varepsilon = 26.6\%$. (The RA are marked in red, the α -bcc phases are marked blue, the low angle grain boundaries are drawn by white lines, the high angle grain boundaries are drawn by black lines.) (Color figure online)

by black lines. As shown in Fig. 8(a, b), majority of the large blocky RA at the ferrite grain boundary transformed to martensite during the initial stage of dynamic deformation ($\varepsilon \leq 5.2\%$). With the increase of strain ($5.2 < \varepsilon \leq 10.3\%$), the RA with smaller average grain size transformed to martensite (Fig. 8c, d). Near the end of deformation, only a few small granular RA that were too stable did not transform (Fig. 8e, f).

Figure 9 shows XRD patterns and the statistical results of RA content in the experimental steel under different strain after quasi-static (strain rate of 0.01 s^{-1}) and dynamic (strain rate of 100 s^{-1}) tensile deformation. It can be seen from Fig. 9 that during the initial stage of tensile deformation ($\varepsilon \leq 5.2\%$), the transformation amount of RA was $\sim 3.9\%$ under dynamic tensile deformation, which was slightly less than $\sim 4.5\%$ under quasi-static tensile deformation. With the increase of strain ($5.2 < \varepsilon \leq 10.3\%$), the transformation amount of RA increased from ~ 3.9 to $\sim 6.4\%$ under dynamic tensile deformation, while it increased from 4.5 to 7.2% during quasi-static tensile deformation. After dynamic and quasi-static tensile

deformation, the transformation amount of RA was ~ 9.7 and $\sim 10.2\%$, respectively.

4. Discussion

4.1 Effect of Strain Rate on Microstructural Evolution

As shown in Fig. 5(b, d, f, h), a large number of dislocations were present in the ferrite grains of experimental steel after tensile deformation at different strain rates. However, the dislocation density in ferrite was relatively low at strain rate of 0.01 s^{-1} (quasi-static deformation) (Fig. 5b). With the increase of strain rate to $10\text{-}200 \text{ s}^{-1}$ (dynamic deformation), the deformation speed was extremely fast, the proliferation of dislocations in a short deformation time made the dislocation slide difficult, resulting in significant increase in dislocation density in ferrite and the density of dislocation tangles and interaction was stronger (Fig. 5d, f, h). Simultaneously, it can be observed from Fig. 5(a, c, e, g) that RA transformed to

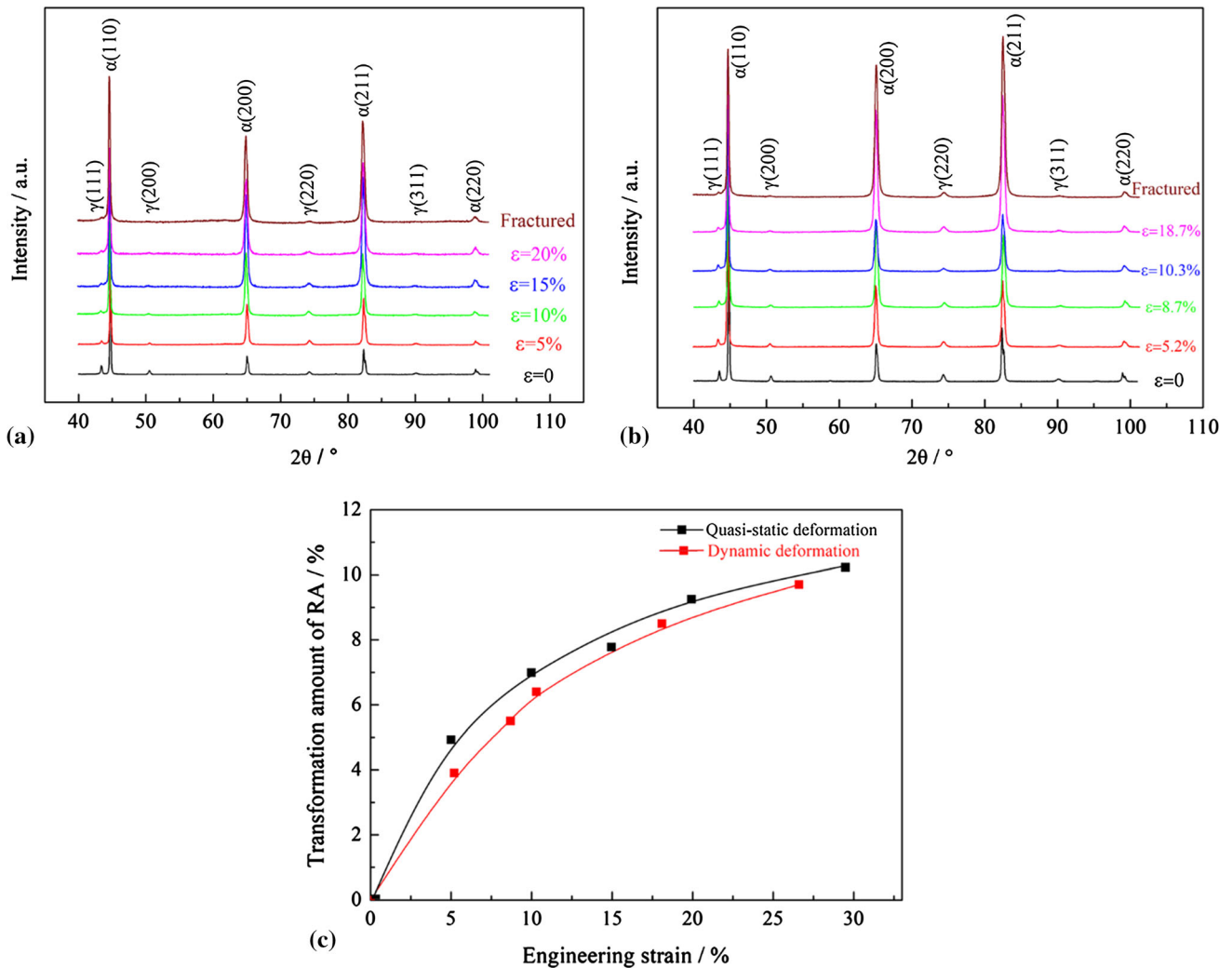


Fig. 9 XRD patterns of the experimental steel under different strain (a) after quasi-static tensile deformation (strain rate of 0.01 s^{-1}), (b) after dynamic tensile deformation (strain rate of 100 s^{-1}) and (c) the statistical results of RA contents

martensite after tensile deformation at different strain rates. According to Figs. 8 and 9, the transformation amount of RA was larger during the initial stage of deformation, irrespective of whether the process was quasi-static or dynamic tensile deformation. This is because the large blocky RA with lower stability is prone to transform to martensite (Ref 21). It should be also noted that with the strain rate increasing from 0.01 to 200 s^{-1} , the transformation of RA into martensite was suppressed gradually (Fig. 8) and the transformation rate of RA in quasi-static tensile deformation was higher than that in dynamic tensile deformation (Fig. 9), which is because of different stabilities of RA during quasi-static and dynamic tensile deformation. This is discussed in section 4.2.

4.2 Effect of Strain Rate on the Stability of RA

The thermodynamic stability of austenite and martensite is presented in Fig. 10 (Ref 22). M_s is the temperature, at which martensite starts to form at pre-existing nucleation sites during cooling, driven by the difference in the chemical free energy $\Delta G_{M_s}^{\gamma \rightarrow \alpha'}$ of austenite and martensite (Ref 23). Assuming that the critical driving force needed to trigger martensitic transformation remained constant over the temperature range of interest,

the martensitic transformation can also occur at temperature T_1 (below T_0 but above M_s) under the required additional mechanical driving force U' , if this additional driving force added to the chemical driving force $\Delta G_{T_1}^{\gamma \rightarrow \alpha'}$ equals $\Delta G_{M_s}^{\gamma \rightarrow \alpha'}$, i.e., $U' + \Delta G_{T_1}^{\gamma \rightarrow \alpha'} = \Delta G_{M_s}^{\gamma \rightarrow \alpha'}$.

For high-speed tensile tests (strain rate ranging from 10 to 200 s^{-1}), the temperature of experimental sample was significantly increased due to adiabatic heating. According to our previous study (Ref 24) and Curtze et al. (Ref 25), the adiabatic temperature rise (ΔT) can be estimated using the following equation:

$$\Delta T = \frac{\Delta Q}{\rho C_p} = \frac{\beta}{\rho C_p} \int_{\epsilon_1}^{\epsilon_2} \sigma d\epsilon$$

where ΔQ is the fraction of mechanical energy that is converted to heat energy, $\rho = 7.8 \text{ gcm}^{-3}$ is the density of steel, $C_p = 0.46 \text{ kJ(kgK)}^{-1}$ is the typical heat capacity of steel, $\beta = 0.9$ is a coefficient related to the fraction of mechanical energy that is converted to heat energy, σ is the true stress, and ϵ is the true strain. The total mechanical energy generated during tensile test was obtained by integrating the area under the σ - ϵ curve.

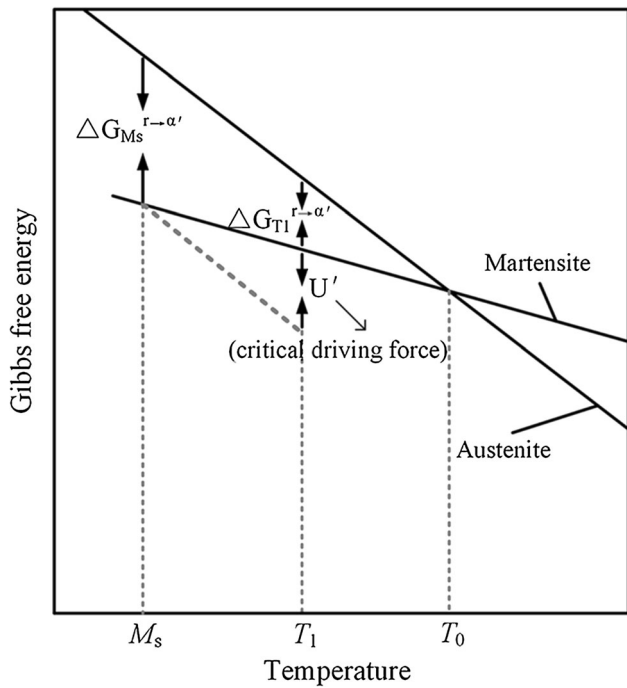


Fig. 10 Free energy of austenite and martensite as a function of temperature

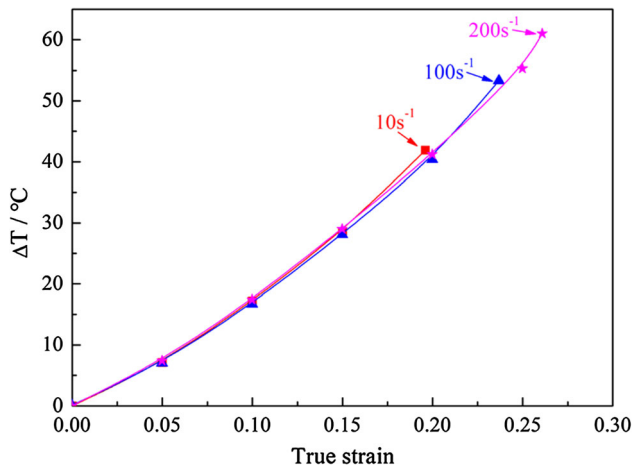


Fig. 11 The estimated ΔT as a function of true strain of the experimental steel deformed at different strain rates

Figure 11 shows the ΔT -true strain (ϵ) curve of the experimental steel deformed at the strain rate ranging from 10 to 200 s^{-1} . Corresponding to strain rate of 10, 100 and 200 s^{-1} , ΔT reached 41, 53 and 61 $^{\circ}C$, respectively. As depicted in Fig. 10, the $\Delta G_{T_1}^{r \rightarrow \alpha'}$ for martensitic transformation decreased with the increase of ΔT , and consequently the required additional U' increased. This is the reason why the RA stability increased with the increase of strain rate.

4.3 Effect of Strain Rate on Mechanical Properties

Considering Fig. 3 and Table 1, it can be seen that YS and UTS increased with the increase of strain rate from 0.01 to 200 s^{-1} , which is in agreement with Choi et al's (Ref 15), Van Slycken et al's (Ref 16) and Wei et al's (Ref 17) results. This is

mainly because the dislocation slide becomes difficult and ferrite is strengthened at higher strain rate (Fig. 5). It may be noted that with the strain rate increasing from 0.01 to 200 s^{-1} , UTS increases by 45 MPa, which is lower than the increase of YS (62 MPa). The possible reason is that the temperature was increased because of adiabatic heating during high-rate deformation, resulting in softening of the matrix (Fig. 11). However, with increase of strain rate from 0.01 to 10 s^{-1} , the TEL decreased from 29.7 to 21.7%. This can be ascribed to two aspects. First, with increase of strain rate from 0.01 to 10 s^{-1} , the amount of transformation of RA decreased insignificantly from 10.2 to 10%, meaning a weak TRIP effect (Fig. 6b). Second, according to He et al. (Ref 19) the significant multiplication of dislocations during the short deformation time made the dislocation slide difficult during dynamic tensile deformation, resulting in deformation localization and causing loss in TEL. As the strain rate was increased from 10 to 200 s^{-1} , the TEL increased from 21.7 to 29.8%. The main reason is that the adiabatic heating started to play an important role in high strain rate. As shown in Fig. 11, with the strain rate increasing from 10 to 200 s^{-1} , the ΔT increased from 41 to 61 $^{\circ}C$, which caused the thermal softening and resulted in the increase of TEL.

5. Conclusions

In this study, the effect of strain rate on microstructural evolution and mechanical properties of the Fe-1.47Mn-1.40Si-0.21C-0.025Nb TRIP steel was elucidated. Additionally, an original tensile specimen with variable cross-section was adopted to realize the controllable strain experiment and study the dynamic deformation process in Fe-1.47Mn-1.40Si-0.21C-0.025Nb TRIP steel. The main conclusions are as follows:

- (1) Compared with quasi-static tensile deformation, the dislocation density in the experimental steel during dynamic tensile deformation was significantly higher, and the density of dislocation tangles and interaction was stronger. However, the transformation amount and the transformation rate of RA at dynamic tensile deformation was less than the quasi-static tensile deformation.
- (2) With the strain rate increasing from 0.01 to 200 s^{-1} , the transformation amount of RA in the steel decreased from 10.2 to 9.2%, owing to the increased adiabatic temperature during dynamic tensile deformation, which led to the increase of required mechanical driving force for the transformation of RA.
- (3) The microstructure of experimental steel was mainly composed of polygonal ferrite, bainite and RA, and majority of large blocky RA at the ferrite grain boundary transformed to martensite during the initial stage of dynamic deformation. With the increase of strain, RA with smaller average grain size transformed to martensite. At the end of deformation, only a few small granular RA that were too stable did not transform.
- (4) With the strain rate increasing from 0.01 to 200 s^{-1} , the YS and UTS of experimental steel increased monotonously from 552 to 614 MPa and 815 to 860 MPa, respectively. However, the TEL (PSE) first decreased from 29.7 to 21.7% (24.2-17.9 GPa%) with the strain rate increasing from 0.01 to 10 s^{-1} , and then increased

to 29.8% (25.6 GPa%) when the strain rate was increased to 200 s^{-1} .

Acknowledgments

The research was supported by the National Natural Science Foundation of China (Grant No. 51874088), Fundamental Research Funds for the Central Universities (Grant No. N2002015), Natural Science Foundation of Fujian Province [No. 2021J05224] and Scientific Research Foundation of Fujian University of Technology (GY-Z21009). The authors are grateful to Dr. R.D.K. Misra for helpful discussion and continued collaboration.

Data Availability

The raw/processed data required to reproduce these findings cannot be shared at this time as the data also form part of an ongoing study.

References

1. W. Shi, L. Li, C.X. Yang, R.Y. Fu, L. Wang and P. Wollants, Strain-Induced Transformation of Retained Austenite in Low-Carbon Low-Silicon TRIP Steel Containing Aluminum and Vanadium, *Mater. Sci. Eng. A*, 2006, **429**(1–2), p 247–251.
2. E. Jimenez-Melero, N.H.V. Dijk, L. Zhao, J. Sietsma, S.E. Offerman, J.P. Wright and S.V. Zwaag, Characterization of Individual Retained Austenite Grains and Their Stability in Low-Alloyed TRIP Steels, *Acta Mater.*, 2007, **55**(20), p 6713–6723.
3. H.J. Jun, S.H. Park, S.D. Choi and C.G. Park, Decomposition of Retained Austenite during Coiling Process of Hot Rolled TRIP-Aided Steels, *Mater. Sci. Eng. A*, 2004, **379**(1–2), p 204–209.
4. J.N. Huang, Z.Y. Tang, H. Ding, H. Zhang, L.L. Bi and R.D.K. Misra, Combining a Novel Cyclic Pre-quenching and Two-Stage Heat Treatment in a Low-Alloyed TRIP-Aided Steel to Significantly Enhance Mechanical Properties Through Microstructural Refinement, *Mater. Sci. Eng. A*, 2019, **764**, 138231.
5. J. Hu, L.X. Du, W. Xu, J.H. Zhai, Y. Dong, Y.J. Liu and R.D.K. Misra, Ensuring Combination of Strength, Ductility and Toughness in Medium-Manganese Steel Through Optimization of Nano-Scale Metastable Austenite, *Mater. Charact.*, 2018, **136**, p 20–28.
6. J. Hu, J.M. Zhang, G.S. Sun, L.X. Du, Y. Liu, Y. Dong and R.D.K. Misra, High Strength and Ductility Combination in Nano-/Ultrafine-Grained Medium-Mn Steel by Tuning the Stability of Reverted Austenite Involving Intercritical Annealing, *J. Mater. Sci.*, 2019, **54**, p 6565–6578.
7. E.M. Bellhouse and J.R. McDermid, Effect of Continuous Galvanizing Heat Treatments on the Microstructure and Mechanical Properties of High Al-Low Si Transformation Induced Plasticity Steels, *Metall. Mater. Trans. A*, 2010, **41**, p 1460–1473.
8. T. Hojo, E. Akiyama, H. Saitoh, A. Shiro, R. Yasuda, T. Shobu, J. Kinugasa and F. Yuse, Effects of Residual Stress and Plastic Strain on Hydrogen Embrittlement of a Stretch-Formed TRIP-Aided Martensitic Steel Sheet, *Corros. Sci.*, 2020, **177**, 108957.
9. A.N. Vasilakos, J. Ohlert, K. Giasla, G.N. Haidemenopoulos and W. Bleck, Low-alloy TRIP steels: A Correlation Between Mechanical

- Properties and the Retained Austenite Stability, *Steel Res. Int.*, 2002, **73**(6–7), p 249–252.
10. J.Y. Choi, J. Lee, K. Lee, J.Y. Koh, J.H. Cho, H.N. Han and K.T. Park, Effects of the Strain Rate on the Tensile Properties of a TRIP-Aided Duplex Stainless Steel, *Mater. Sci. Eng. A*, 2016, **666**, p 280–287.
 11. J.V.T. Kumar, J. Sudha, K.A. Padmanabhan, A.V. Frolova and V.V. Stolyarov, Influence of Strain Rate and Strain at Temperature on TRIP Effect in a Metastable Austenitic Stainless Steel, *Mater. Sci. Eng. A*, 2020, **777**, 139046.
 12. P. Verleysen, J. Peirs, J. Van Slycken, K. Faes and L. Duchene, Effect of Strain Rate on the Forming Behaviour of Sheet Metals, *J. Mater. Process. Technol.*, 2011, **211**, p 1457–1464.
 13. Z.H. Cai, D.L. Zhang, L.F. Ma, H. Ding, Y. Feng, J. Hu and R.D.K. Misra, Competing Deformation Mechanisms in an Austenite-Ferrite Medium-Mn Steel at Different Strain Rates, *Mater. Sci. Eng. A*, 2021, **818**, 141357.
 14. O. Grössl, L. Krüger, G. Frommeyer and L.W. Meyer, High Strength Fe-Mn-(Al, Si) TRIP/TWIP Steels Development-Properties-Application, *Int. J. Plast.*, 2000, **16**(10–11), p 1391–1409.
 15. I.D. Choi, D.M. Bruce, S.J. Kim, C.G. Lee, S.H. Park, D.K. Matlock and J.G. Speer, Deformation Behavior of Low Carbon TRIP Sheet Steels at High Strain Rates, *ISIJ Int.*, 2002, **42**(12), p 1483–1489.
 16. J. Van Slycken, P. Verleysen, J. Degrieck, L. Samek and B.C. De Cooman, High-Strain-Rate Behavior of Low-Alloy Multiphase Aluminum- and Silicon-Based Transformation-Induced Plasticity Steels, *Metall. Mater. Trans. A*, 2006, **37**, p 1527–1539.
 17. X.C. Wei, R.Y. Fu and L. Li, Tensile Deformation Behavior of Cold-Rolled TRIP-Aided Steels over Large Range of Strain Rates, *Mater. Sci. Eng. A*, 2007, **465**, p 260–266.
 18. Y. Gao, C. Xu, Z.P. He, Y.L. He and L. Li, Response Characteristics and Adiabatic Heating during High Strain Rate for TRIP Steel and DP Steel, *J. Iron Steel Res. Int.*, 2015, **22**(1), p 48–54.
 19. Z.P. He, Y.L. He, Y.T. Ling, Q.H. Wu, Y. Gao and L. Li, Effect Of Strain Rate on Deformation Behavior of TRIP Steels, *J. Mater. Process. Technol.*, 2012, **212**(10), p 2141–2147.
 20. J.N. Huang, Z.Y. Tang, H. Ding and R.D.K. Misra, The Significant Impact of Phase Fraction and Austenite Stability on the Mechanical Properties of a Low-Alloyed TRIP-Aided Steel: An Insight into Experimental Analysis and Predictions, *Mater. Sci. Eng. A*, 2019, **759**, p 40–46.
 21. C. Wang, H. Ding, M.H. Cai and B. Rolfe, Characterization of Microstructures and Tensile Properties of TRIP-Aided Steels with Different Matrix Microstructure, *Mater. Sci. Eng. A*, 2010, **610**, p 65–75.
 22. S. Curtze, V.T. Kuokkala, M. Hokka and P. Peura, Deformation Behavior of TRIP and DP Steels in Tension at Different Temperatures over a Wide Range of Strain Rates, *Mater. Sci. Eng. A*, 2009, **507**, p 124–131.
 23. G.F. Bolling and R.H. Richman, The Plastic Deformation-Transformation of Paramagnetic F.C.C. Fe-Ni-C Alloys, *Acta Metall.*, 1970, **18**(6), p 673–681. [https://doi.org/10.1016/0001-6160\(70\)90097-0](https://doi.org/10.1016/0001-6160(70)90097-0)
 24. Z.Y. Tang, J.N. Huang, H. Ding, Z.H. Cai and R.D.K. Misra, On the Dynamic Behavior and Relationship to Mechanical Properties of Cold-Rolled Fe-0.2C-15Mn-3Al Steel at Intermediate Strain Rate, *Mater. Sci. Eng. A*, 2019, **742**, p 423–431.
 25. S. Curtze and V.T. Kuokkala, Dependence of Tensile Deformation Behavior of TWIP Steels on Stacking Fault Energy, Temperature and Strain Rate, *Acta Mater.*, 2019, **58**(15), p 5129–5141.

Publisher's Note Springer Nature remains neutral with regard to jurisdictional claims in published maps and institutional affiliations.